Simulated tempering and magnetizing: Application of two-dimensional simulated tempering to the two-dimensional Ising model and its crossover

Tetsuro Nagai[1] and Yuko Okamoto[1,2,3,4]

[1]*Department of Physics, Graduate School of Science, Nagoya University, Nagoya, Aichi 464-8602, Japan*
[2]*Structural Biology Research Center, Graduate School of Science, Nagoya University, Nagoya, Aichi 464-8602, Japan*
[3]*Center for Computational Science, Graduate School of Engineering, Nagoya University, Nagoya, Aichi 464-8603, Japan*
[4]*Information Technology Center, Nagoya University, Nagoya, Aichi 464-8601, Japan*

(Received 10 May 2012; published 9 November 2012)

We have performed two-dimensional simulated tempering (ST) simulations of the two-dimensional Ising model with different lattice sizes in order to investigate the two-dimensional ST's applicability to dealing with phase transitions and study the crossover of critical scaling behavior. The external field, as well as the temperature, was treated as a dynamical variable updated during the simulations. Thus this simulation can be referred to as simulated tempering and magnetizing (STM). We also performed simulated magnetizing (SM) simulations, in which the external field was considered as a dynamical variable and temperature was not. As discussed in previous studies, the ST method is not always compatible with first-order phase transitions. This is also true in the magnetizing process. Flipping of the entire magnetization did not occur in the SM simulations under the critical temperature T_c in large-lattice-size simulations; however, the phase changed through the high-temperature region in the STM simulations. Thus the dimensional extension let us eliminate the difficulty of the first-order phase transitions and study a wide area of the phase space. We discuss how frequently parameter-updating attempts should be made for optimal convergence. The results favor frequent attempts. We finally study the crossover behavior of the phase transitions with respect to the temperature and external field. The crossover behavior is clearly observed in the simulations, in agreement with the theoretical implications.

DOI: 10.1103/PhysRevE.86.056705 PACS number(s): 05.10.Ln, 64.60.De, 75.30.Kz, 75.10.Hk

I. INTRODUCTION

In the computational statistical physics field, Monte Carlo (MC) and molecular dynamics simulations have been commonly used. However, the quasiergodicity problem, where simulations tend to get trapped in states of energy local minima, has often posed great difficulty. In order to overcome this difficulty, generalized-ensemble algorithms have been developed and applied to many systems including spin systems and biomolecular systems (for reviews, see, e.g., Refs. [1–3]).

Commonly used examples of generalized-ensemble algorithms are the multicanonical algorithm (MUCA) [4,5], simulated tempering (ST) method [6,7], and replica-exchange method (REM) [8,9] (it is also referred to as parallel tempering). Closely related to the MUCA are the Wang-Landau method [10,11] and metadynamics [12]; closely related to the REM is the method in Ref. [13].

In the ST method, temperature is regarded as a dynamical variable, which is updated by the Metropolis criterion during the simulation and consequently a random walk is realized in the temperature space. This random walk in turn causes a random walk of the energy, which enables the system in question to overcome free-energy barriers. However, it is well known that the ST method is not very compatible with first-order phase transitions (for a review, see, e.g., Ref. [14]). When there is a first-order phase transition, the random walk of temperature across the phase-transition point hardly occurs. We remark that there has been a recent attempt to deal with this difficulty by an extension of ST [15].

Recently, the multidimensional generalizations of the generalized-ensemble algorithms, including the MUCA, ST, and REM, were discussed and general formalisms were given [16–18]. In these methods, the energy of the system is generalized by adding other energy term or terms with some coupling constants. In the multidimensional ST method, not only the temperature but also the coupling constants are considered as dynamical variables.

In this work we study a special case of the above general multidimensional ST methods. Namely, the additional term is $-hM$, where h and M are the external field and the magnetization, respectively. The external field h corresponds to the coupling constant that is updated during MC simulations. Therefore, not only temperature but also external field becomes a dynamical variable and is expected to realize a random walk during the simulations. Thus this simulation can be referred to as simulated tempering and magnetizing (STM). In order to test the effectiveness of the present method, we applied it to the two-dimensional Ising model.

The Ising model has two kinds of phase transitions. One occurs with the change of temperature when the external field is zero. The other occurs with the change of the external field when the temperature is under the critical temperature T_c. The former is classified as a second-order phase transition. The latter is categorized as a first-order phase transition unless the temperature is exactly equal to T_c. When $T = T_c$ the transitions are classified as second-order phase transitions. This system allows us to confirm the applicability of the two-dimensional ST to the first-order phase transitions with the external field changes.

We also investigate the crossover phenomena in the phase transitions, in which critical exponents are changed. We study the behavior of magnetization per spin m, which follows $m \sim |T - T_c|^{\beta}$ and $m \sim |h|^{1/\delta}$ near the critical point, where β and δ are critical exponents [19]. Our simulation method, with a combination of histogram reweighting techniques, enables us to calculate physical values such as the energy

and magnetization at various values of T and h from a single production run.

This article is organized as follows. In Sec. II we present the STM method. In Sec. III we present the results. Section IV is devoted to conclusions.

II. MATERIALS AND METHODS

A. System

We study the two-dimensional Ising model in an external field. The total energy is given by

$$H = E - hM, \tag{1}$$

$$E = -\sum_{\langle i,j\rangle} \sigma_i \sigma_j, \tag{2}$$

$$M = \sum_{i=1}^{N} \sigma_i, \tag{3}$$

where i, N, σ_i, and h are the index of spin, the total number of spins, the spin at the ith site, and the external field, respectively. The spin σ_i takes on the values ± 1. The sum in Eq. (2) goes over the nearest-neighbor pairs. The spins are arranged on a square $L \times L$ lattice. We impose periodic boundary conditions. Data were obtained for lattice sizes from 2×2 to 160×160.

B. Simulation methods

Whereas the conventional ST method considers temperature as a dynamical variable, the STM method considers not only temperature but also external field as a dynamical variable. Here, before explaining the STM method, we shortly review the conventional ST method [6,7].

In the conventional ST method, temperature is a dynamical variable that takes on one of the N_T values (here temperature is discretized into N_T values). In other words, denoting by X and x a sampling space and its microscopic state, respectively, the Boltzmann factor

$$e^{-E(x)/T + a(T)} \tag{4}$$

is regarded as a joint probability for the state (x,T) $(\in X \otimes \{T_1, T_2, \ldots, T_{N_T}\})$. Here $a(T)$ [or $a(T_i)$] is a parameter for obtaining uniform distributions of temperature values. Here and hereafter, we set Boltzmann's constant to unity. Now that the temperature is a dynamical variable, the simulated system is allowed to realize a random walk in the temperature space. This random walk in turn causes a random walk of energy. Consequently, the simulated system has more chance to overcome energy barriers.

Even though temperature changes during ST simulations, any thermodynamic quantity at temperature T_i, $\langle A\rangle_{T_i}$, can be reconstructed with the conditional expectation of a physical quantity A given at T_i, or $\langle A|T_i\rangle$. Note that

$$\begin{aligned}\langle A|T_i\rangle_{\mathrm{ST}} &= \frac{\sum_{j=1}^{N_T} \int dx\, A(x)\delta_{ij} \exp\left(-\frac{E(x)}{T_j} + a(T_j)\right)}{\sum_{j=1}^{N_T} \int dx\, \delta_{ij} \exp\left(-\frac{E(x)}{T_j} + a(T_j)\right)} \\ &= \frac{\int dx\, A(x) \exp\left(-\frac{E(x)}{T_i} + a(T_i)\right)}{\int dx \exp\left(-\frac{E(x)}{T_i} + a(T_i)\right)} \\ &= \langle A\rangle_{T_i}, \end{aligned} \tag{5}$$

where δ_{ij} is the Kronecker delta. Namely, we have

$$\langle A\rangle_{T_i} = \frac{1}{N_{T_i}} \sum_{j=1}^{N_{T_i}} A_{T_i}^{j}, \tag{6}$$

where N_{T_i} and $A_{T_i}^{j}$ stand for the total number of samples and the jth sample at T_i.

To find a candidate for $a(T_i)$, let us look at the probability of visiting T_i. By summing over the delta function, the probability of occupying T_i is given by

$$\begin{aligned} P(T_i) &= \frac{\sum_{j=1}^{N_T} \int dx\, \delta_{ij} \exp\left(-\frac{E(x)}{T_j} + a(T_j)\right)}{\sum_{j=1}^{N_T} \int dx \exp\left(-\frac{E(x)}{T_j} + a(T_j)\right)} \\ &= \frac{e^{-f(T_i)+a(T_i)}}{\sum_{j=1}^{N_T} e^{-f(T_j)+a(T_j)}} \\ &\propto e^{-f(T_i)+a(T_i)}, \end{aligned} \tag{7}$$

where f is the dimensionless (Helmholtz) free energy and

$$e^{-f(T)} \equiv \int dx\, e^{-E(x)/T}. \tag{8}$$

Substituting $f(T_i)$ into $a(T_i)$ gives constant probability regardless of T_i. Thus the dimensionless free energy $f(T_i)$ is a good choice for $a(T_i)$ to obtain a uniform temperature distribution and realize a random walk in the temperature space. Although the free energy is not known *a priori*, unless the system is exactly solvable, the free-energy calculation methods (the details will be provided below) enable us to get a good estimate from preliminary simulation runs.

In the two-dimensional ST algorithm, in contrast, we consider that another parameter is also a dynamical variable [16–18]. Particularly in the STM method, the external field h is a second dynamical variable. In other words, we consider

$$e^{-(E-hM)/T + a(T,h)} \tag{9}$$

as a joint probability for (x,T,h) $(\in X \otimes \{T_1, T_2, \ldots, T_{N_T}\} \otimes \{h_1, h_2, \ldots h_{N_h}\})$, where $a(T,h)$ is a parameter.

To find a candidate for $a(T_i,h_j)$, we again look at the probability of staying at each set of parameter values. It is given by

$$\begin{aligned} &P(T_i,h_j) \\ &= \frac{\sum_{k=1}^{N_T}\sum_{l=1}^{N_h} \int dx\, \delta_{ik}\delta_{jl} \exp\left(-\frac{E(x)-h_l M(x)}{T_k} + a(T_k,h_l)\right)}{\sum_{k=1}^{N_T}\sum_{l=1}^{N_h} \int dx \exp\left(-\frac{E(x)-h_l M(x)}{T_k} + a(T_k,h_l)\right)} \\ &= \frac{e^{-f(T_i,h_j)+a(T_i,h_j)}}{\sum_{k=1}^{N_T}\sum_{l=1}^{N_h} e^{-f(T_k,h_l)+a(T_k,h_l)}} \\ &\propto e^{-f(T_i,h_j)+a(T_i,h_j)}, \end{aligned} \tag{10}$$

where

$$e^{-f(T_i,h_j)} = \int dx\, e^{-(E-h_j M)/T_i}. \tag{11}$$

The dimensionless free energy $f(T_i,h_j)$ is again a good choice for $a(T_i,h_j)$ to acquire a uniform distribution of T and h. These values can be estimated from preliminary simulation runs and reweighting techniques.

As in the conventional ST method, any thermal average $\langle A\rangle_{T_i,h_j}$ at given T_i $(\in \{T_1, T_2, \ldots, T_{N_T}\})$ and

TABLE I. Conditions of the two-dimensional ST simulations.

Lattice size L	2, 4, 8, 10, 20	30	80	160
Number of production runs	1	2	4	2
Total MC sweeps per run	42000000	42000000	1000000000	321300000
Parameter-updating period	50	20	10	5
T_1–T_{N_T}	1.0–5.0	1.0–5.0	1.0–5.0	1.0–3.6
h_1–h_{N_h}	−1.5–1.5	−1.5–1.5	−1.5–1.5	−0.5–0.5
N_T	20	20	70	63
N_h	21	21	51	51
N_{data}[a]	10	10	100	50

[a]The data were stored every N_{data} MC sweeps.

h_j ($\in \{h_1, h_2, \ldots, h_{N_h}\}$) can be obtained by calculating the conditional expectation $\langle A\rangle_{T_i,h_j} = \langle A|T_i,h_j\rangle_{\text{ST}}$. Namely, we have

$$\langle A\rangle_{T_i,h_j} = \frac{1}{N_{T_i,h_j}} \sum_{k=1}^{N_{T_i,h_j}} A^k_{T_i,h_j}, \tag{12}$$

where N_{T_i,h_j} is the total number of samples at T_i and h_j, and $A^k_{T_i,h_j}$ stands for the kth sample at T_i and h_j.

The method of updating T or h is similar to that of updating spins because T and h are considered as dynamical variables. The Metropolis criterion for updating T or h is given by the following transition probability:

$$\begin{aligned} &w(T_i,h_j \to T_{i'},h_{j'}) \\ &= \min\left(1, \frac{P(T_{i'},h_{j'})}{P(T_i,h_j)}\right) \\ &= \min\left\{1, \exp\left[-\left(\frac{1}{T_{i'}} - \frac{1}{T_i}\right)E + \left(\frac{h_{j'}}{T_{i'}} - \frac{h_j}{T_i}\right)M \right.\right. \\ &\quad \left.\left. + a(T_{i'},h_{j'}) - a(T_i,h_j)\right]\right\}. \end{aligned} \tag{13}$$

Once an initial state is given, the STM simulations can be performed by repeating the following two steps. (i) We perform a conventional canonical simulation at T_i and h_j for certain MC sweeps. (ii) We update the temperature or external field by Eq. (13) with $a(T,h) = f(T,h)$.

In our implementation, every certain MC sweeps either T or h was updated (the choice between T and h was made at random) by Eq. (13) to a neighboring value (the choice of two neighbors was also made at random). Here one MC sweep stands for $L \times L$ single-spin updates. The number of MC sweeps performed between parameter updates is here referred to as the parameter-updating period.

Whereas updating the parameter to a neighboring value with the Metropolis algorithm should be considered the easiest to implement, we remark that, as spins can be updated by a number of methods such as the heat bath method, other schemes of updating the parameters can be employed [20]. There also exists a temperature updating scheme for ST by the Langevin algorithm [21].

Table I summarizes the conditions of the present simulations. For $L = 80$, instead of a single 4 000 000 000 MC sweep production run, four 1 000 000 000 MC sweep runs were performed. This was just to make one trajectory shorter and easier to deal with numerically. Similarly, two production runs (instead of a single run) were made for $L = 30$ and 160.

As for spin updates, we employed the single-spin-update algorithm; we updated spins one by one with the Metropolis criterion. As for a quasi-random-number generator, we used the Mersenne twister [22].

C. Free-energy calculations

The simulated tempering parameters, or free energy in Eqs. (9) and (11), can be simply obtained by the reweighting techniques applied to the results of preliminary simulation runs [16–18,23]. We employed two reweighting methods for this free-energy calculation. One method is the multiple-histogram reweighting method, or weighted histogram analysis method (WHAM) [24,25], and the other is the multistate Bennett acceptance ratio (MBAR) estimator [26], which is based on the WHAM.

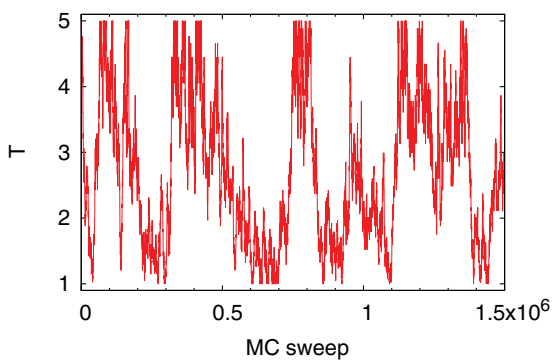

FIG. 1. (Color online) History of the temperature T. The linear lattice size L is 80.

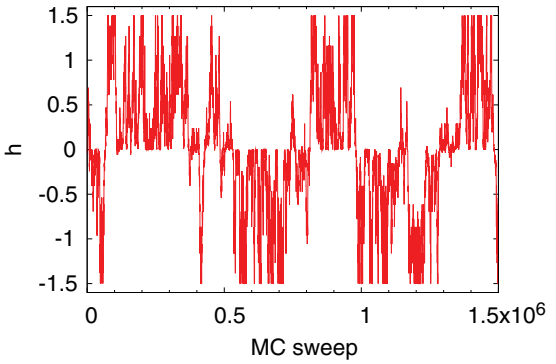

FIG. 2. (Color online) History of the external field h. The linear lattice size L is 80.

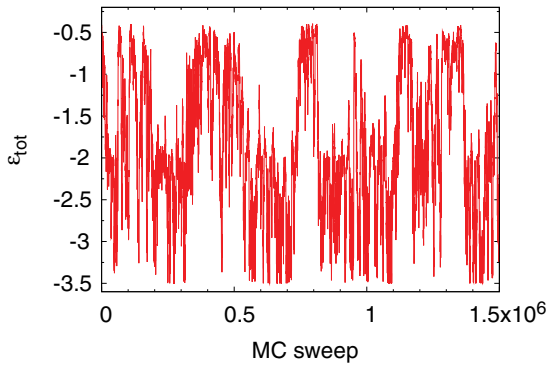

FIG. 3. (Color online) History of the total energy per spin $\epsilon_{\rm tot}$. The linear lattice size L is 80.

The equations of the WHAM algorithm that were applied to the simulation results are as follows. For details, the reader is referred to Refs. [17,25]. The density of states (DOS) $n(E,M)$ and free-energy values $f(T_i,h_j)$ can be obtained by

$$n(E,M)=\frac{\sum_{T_i,h_j} n_{T_i,h_j}(E,M)}{\sum_{T_i,h_j} N_{T_i,h_j}\exp[f(T_i,h_j)-(E-h_jM)/T_i]}, \tag{14}$$

$$f(T_i,h_j)=-\ln\sum_{E,M} n(E,M)\exp[-(E-h_jM)/T_i], \tag{15}$$

where $n_{T_i,h_j}(E,M)$ is the histogram of E and M at T_i and h_j, and N_{T_i,h_j} is the total number of samples obtained at T_i and h_j. By solving these two equations self-consistently by iterations, we can obtain $n(E,M)$ and $f(T_i,h_j)$. The obtained $n(E,M)$ allows one to calculate any thermal average at arbitrary temperature and external field values. Note that $f(T_i,h_j)$ is determined up to a constant, which sets the zero point of the free energy. Accordingly, $n(E,M)$ is determined up to a normalization constant.

The MBAR estimator is based on the following equations. Namely, by combing Eqs. (14) and (15), the free energy can be written as

$$f(T_i,h_j)=-\ln\sum_{n=1}^{N}\frac{\exp[-(E_n-h_jM_n)/T_i]}{\sum_{k=1}^{N_T}\sum_{l=1}^{N_h} N_{T_k,h_l}\exp[f(T_k,h_l)-(E_n-h_lM_n)/T_k]}, \tag{16}$$

where N, N_{T_k,h_l}, E_n, and M_n are the total number of data, the number of samples associated with T_k and h_l, the energy of the nth data, and the magnetization of the nth data, respectively. This equation should be solved self-consistently for $f(T_i,h_j)$. Note that, as in the WHAM, $f(T_i,h_j)$ is determined up to a constant.

We repeat the preliminary STM simulations and free-energy calculations until we finally obtain sufficiently accurate free-energy values that let the system perform a random walk in the temperature and external field space during the STM simulation. We then perform a single, final production run.

Note that these two reweighting methods enable us to obtain not only dimensionless free-energy values but also physical values at any temperature and at any external field, which are given by

$$\langle A\rangle_{T,h}=\sum_{n=1}^{N} W_{na}A(x_n), \tag{17}$$

$$W_{na}=\frac{1}{\langle c_a\rangle}\frac{\exp[-(E_n-hM_n)/T]}{\sum_{k=1}^{N_T}\sum_{l=1}^{N_h} N_{T_k,h_l}\exp f(T_k,h_l)-(E_n-h_lM_n)/T_k]}, \tag{18}$$

$$\langle c_a\rangle=\sum_{n=1}^{N}\frac{\exp[-(E_n-hM_n)/T]}{\sum_{k=1}^{N_T}\sum_{l=1}^{N_h} N_{T_k,h_l}\exp[f(T_k,h_l)-(E_n-h_lM_n)/T_k]}. \tag{19}$$

For details, the reader is referred to Refs. [26,27].

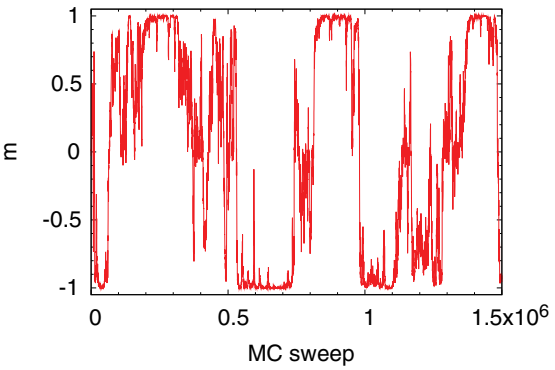

FIG. 4. (Color online) History of the magnetization per spin m ($\equiv M/L^2$). The linear lattice size L is 80.

We also used another method of calculating the free energy. By substituting $a(T,h)$ in Eq. (10) for the estimates for free

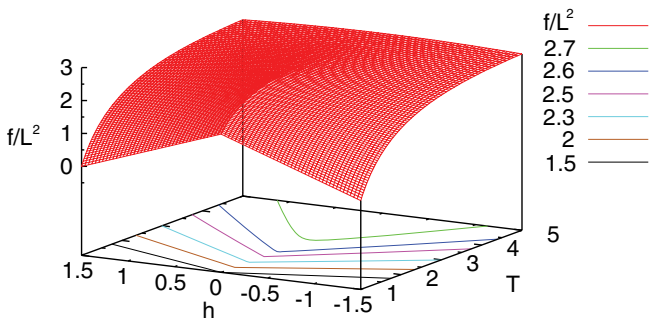

FIG. 5. (Color online) Free energy per spin f/L^2 and its contour curves as functions of T and h. The linear lattice size L is 80.

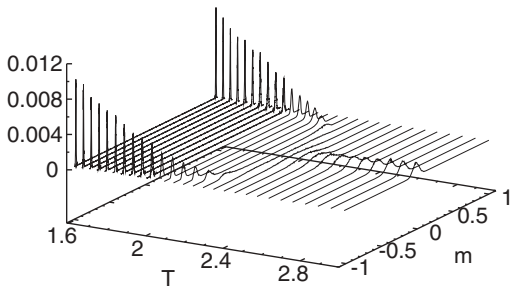

FIG. 6. Distribution of m as a function of T for $h = 0$. The linear lattice size L is 80.

energy $\tilde{f}(T,h)$, we obtain

$$P(T,h) \propto e^{-f(T,h)+\tilde{f}(T,h)}. \tag{20}$$

From this we can write

$$f(T,h) = \tilde{f}(T,h) - \ln P(T,h) + \text{const.} \tag{21}$$

Here $P(T,h)$ can be obtained as the number of samples at each set of parameter values in a preliminary STM simulation. Thus this equation enables one to refine the free energy much more easily than the reweighting methods because the method does not require any iterations. This method does not work well, however, when $P(T_i,h_j)$ is too small [or $\tilde{f}(T_i,h_j)$ is too far away from true values] to obtain samples at (T_i,h_j), while the reweighting techniques are still able to work. In the present work we first use the reweighting methods to obtain rough estimates of the free energy for the entire parameter space. We then use the combination of the reweighting methods and Eq. (21) for further refinements of the free energy.

Note that the WHAM gives another piece of information, namely, the DOS, which the MBAR estimator cannot directly calculate. However, the WHAM requires one to make histograms before iterations and two kinds of calculations in an iteration step. As the system size grows, the number of possible states increases. Thus the calculation of the DOS can be quite time consuming. In contrast, the MBAR estimator can be used without making histograms and one MBAR estimator iteration step needs one equation. The length of one iteration, which is approximately proportional to the number of samples and parameter values, increases and can be time consuming, as the system size is enlarged. However, we have the impression that the MBAR estimator is less time consuming and more easily implemented than the WHAM. The parallelization of the MBAR estimator is slightly easier than that of the WHAM and we actually did it with OpenMP.

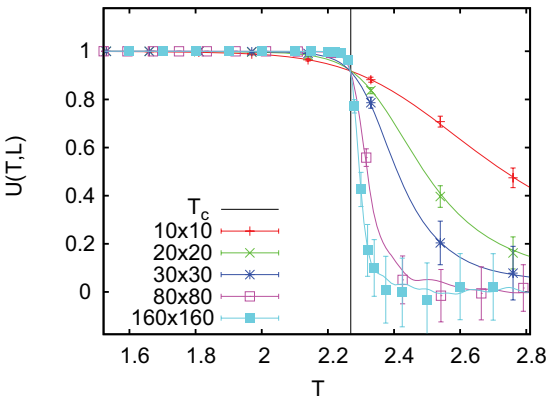

FIG. 8. (Color online) Binder cumulant U vs temperature.

D. Temperature and external field distributions

As mentioned in the preceding sections, we have to give the set of temperature and external field values before ST or STM simulations. Actually, the determination involves trial and error. However, the reweighting methods still help one to do this to a certain extent.

The maximum and minimum values of the temperature and external field were chosen so that the area of the temperature and external field was wide enough to investigate the critical behaviors. This should be done separately for each system and what is to be investigated.

The distribution of temperature was chosen to be proportional to an exponential to the index number in small lattice sizes, as is common in simulated tempering and replica-exchange methods. However, in large-lattice-size systems, we assigned more values around T_c by hand. A denser distribution is required where the heat capacity is large or the phase transition occurs. The distribution of the external field is similarly assigned. In small lattice sizes it was proportional to the index of the external field. However, in the larger lattice sizes we assigned more points around $h = 0$, in which the phase transition occurs. We assigned them in such a manner that the acceptance rate of ST parameter updates are preferably between 10% and 50%. This fuzzy criterion is partly due to the two-dimensional distributions. A temperature distribution at a certain external field does not always give the same acceptance rates under another external field.

When the distributions of T_i and h_j turned out to be improper, we reassigned the distributions. In this case, we already had the samples and free-energy estimates at a previous distribution, with which the reweighting method lets one estimate the free energy at the newly distributed

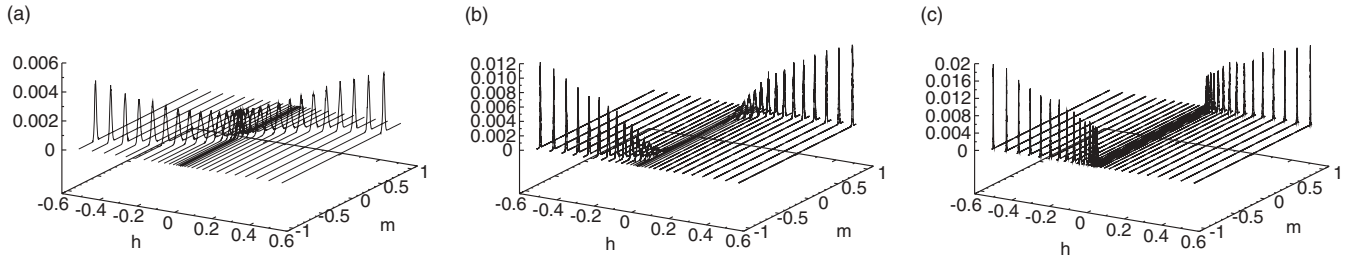

FIG. 7. Distribution of m as a function of h for (a) $T = 3.21$, (b) $T = 2.316$, and (c) $T = 1.967$. The linear lattice size L is 80.

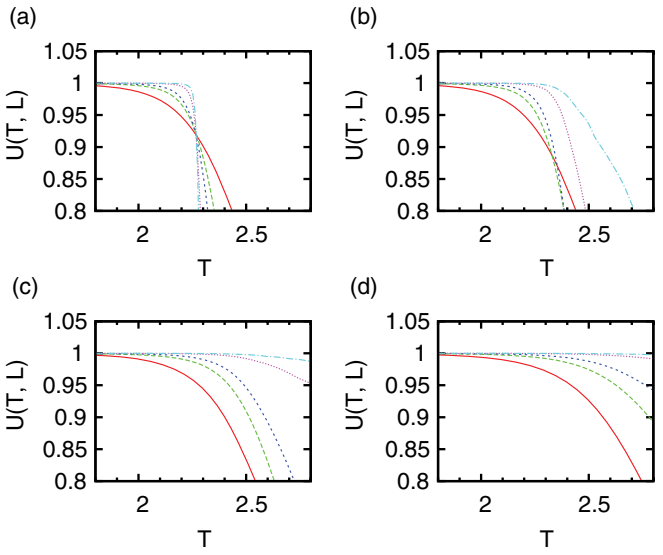

FIG. 9. (Color online) Binder cumulant U vs temperature under different external fields: (a) $h = 0$, (b) $h = 0.01$, (c) $h = 0.05$, and (d) $h = 0.1$. The red solid, dashed green, dark blue short-dashed, purple dotted, and light blue dot-dashed lines stand for $L = 10$, 20, 30, 80, and 160, respectively.

values. Consequently, we did not have to start the free-energy calculations over from the beginning. We actually repeated this parameter redistribution procedure several times, especially in large-lattice-size simulations.

III. RESULTS AND DISCUSSION

A. Simulated tempering and magnetizing simulations

We shall show that the two-dimensional ST simulations were carried out properly. Figures 1 and 2 show the temperature and external field, respectively, as functions of the MC sweep. Both were obtained from the simulations in which the linear lattice size was 80. The temperature and external field indeed realized random walks.

Figures 3 and 4 show the energy and magnetization per spin, respectively, as functions of the MC sweep. They also realized random walks. Note that there are expected correlations between the temperature and energy (see Figs. 1 and 3) and between the external field and magnetization (see Figs. 2 and 4). The same behavior was observed in other-lattice-size simulations (data not shown).

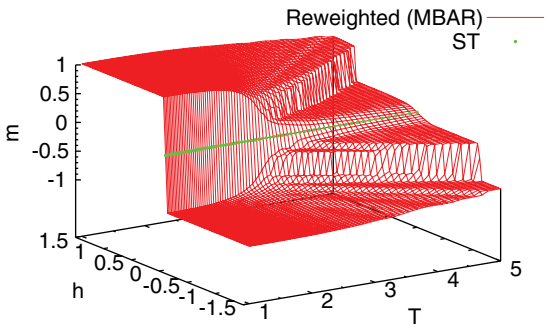

FIG. 10. (Color) Reweighted data (red) and original data (green) obtained by the conventional ST. The linear lattice size L is 80.

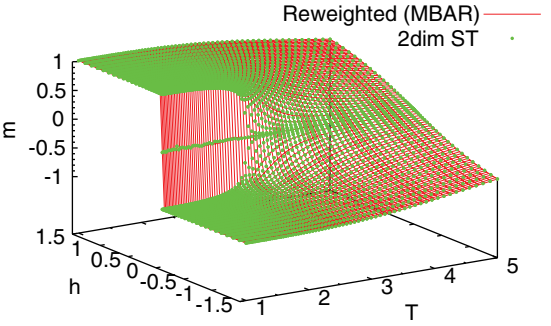

FIG. 11. (Color) Reweighted data (red) and original data (green) obtained by the STM simulations. The linear lattice size L is 80.

Figure 5 shows the dimensionless free energy per spin as a function of temperature and external field, which was obtained by applying the MBAR estimator to the results of the production runs. Note that the partial differential of this free energy by h gives $\frac{\langle m \rangle}{T}$. The shape at $h = 0$ suggests a jump of m below T_c, indicating the existence of the first-order phase transitions.

Figure 6 shows the distribution of magnetization as a function of temperature. Below T_c the distribution is separated into two parts. As temperature increases, the distribution becomes broader. Near T_c the distribution is the broadest and two peaks merge. It then becomes narrower. Note that this figure was obtained by only four production runs (see Table I) and can be obtained even by only one production run, though the error is expected to become larger. Figures 7(a), 7(b), and 7(c) show the distribution of magnetization as a function of external field above, around, and below T_c, respectively. Above T_c the change is smooth and continuous [see Fig. 7(a)]. Around T_c the distribution becomes very wide around $h = 0$ [see Fig. 7(b)]. This is one of the properties of the second-order phase transitions. Below T_c the distribution jumps from one side to the other side at $h = 0$ [see Fig. 7(c)]. This abrupt jump of the distribution is one of the properties of the first-order phase transitions.

We also calculated the Binder cumulant [28] defined by

$$U(T,h,L) \equiv \frac{1}{2}\left(3 - \frac{\langle m^4 \rangle}{\langle m^2 \rangle^2}\right). \tag{22}$$

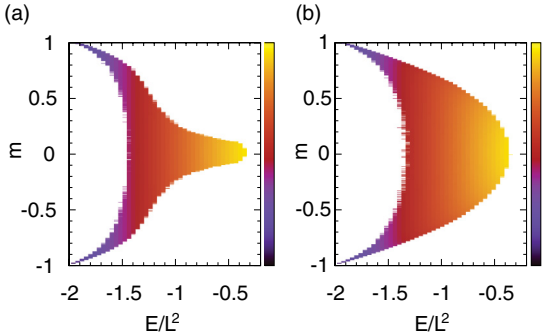

FIG. 12. (Color) Calculated DOS obtained by the WHAM with (a) ST and (b) STM data. The linear lattice size L is 80.

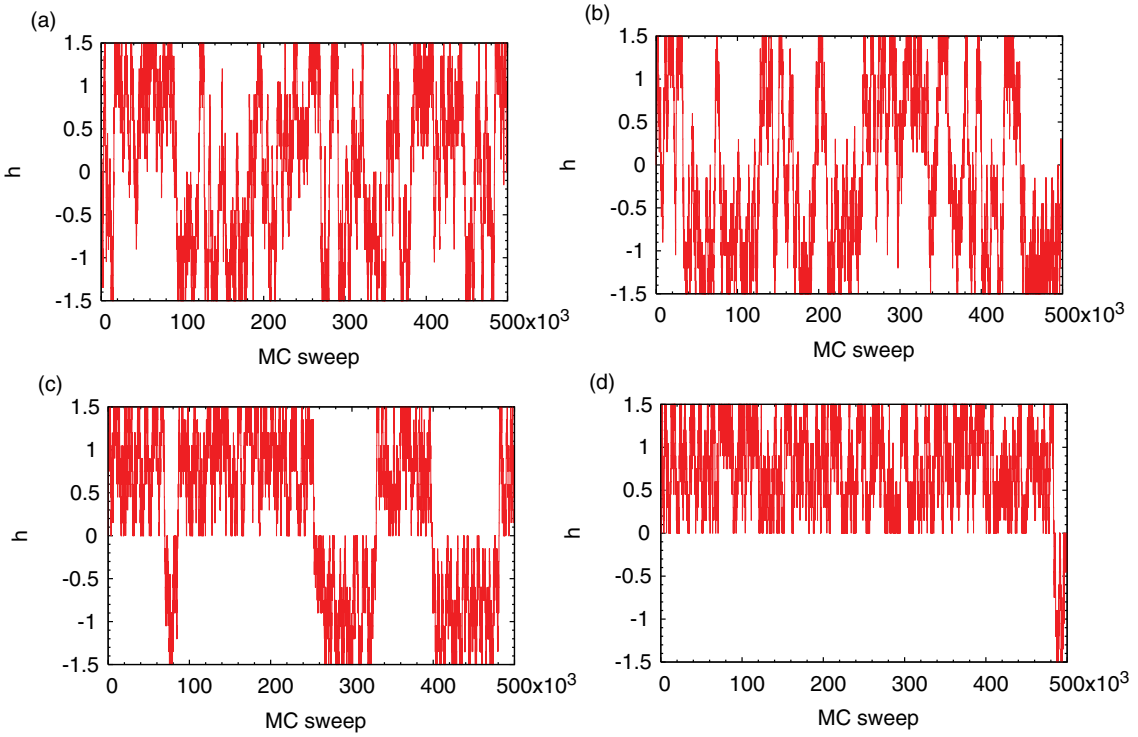

FIG. 13. (Color online) External field vs MC sweep in SM simulations under T_c ($T = 1.97$). The linear lattice size L is (a) 2, (b) 4, (c) 8, and (d) 10, respectively.

Figure 8 shows the Binder cumulant as a function of temperature. As is well known, the graphs cross at one point at T_c. The error bars were obtained by the jackknife method [29,30].

Figure 9 shows the Binder cumulant as a function of temperature under different external fields. The graphs do not cross at one point in the presence of a finite external field. The amount of errors is expected to be on the same level of Fig. 8 and the error bars are suppressed here to aid the eye.

B. Comparison of ST with STM

We compared the results of the STM method with those of the conventional ST method. Figures 10 and 11 show the magnetization as a function of the temperature and external field, which was calculated using the MBAR estimator with the data obtained by the conventional ST and STM simulations, respectively. Figure 10, which was obtained by the conventional ST, shows artifactual jumps at a high temperature and a certain external field. This must have been caused by a failure to sample some parts of states. In contrast, the results by the STM simulations are smooth (see Fig. 11). Figure 12 shows the density of states obtained by conventional ST and STM simulations. This obviously illustrates that the area in which the energy is relatively high with somewhat strong magnetizations was not sampled by the conventional ST method. These results imply that the dimensional extension in the STM enlarged the sampled space.

Once one succeeds in estimating the free-energy values, or ST and STM parameters $a(T_i)$ and $a(T_i,h_j)$, with sufficient accuracy, one can perform ST and STM simulations properly. However, the computational efforts in free-energy calculations are still much larger for STM than for ST. Therefore, it is

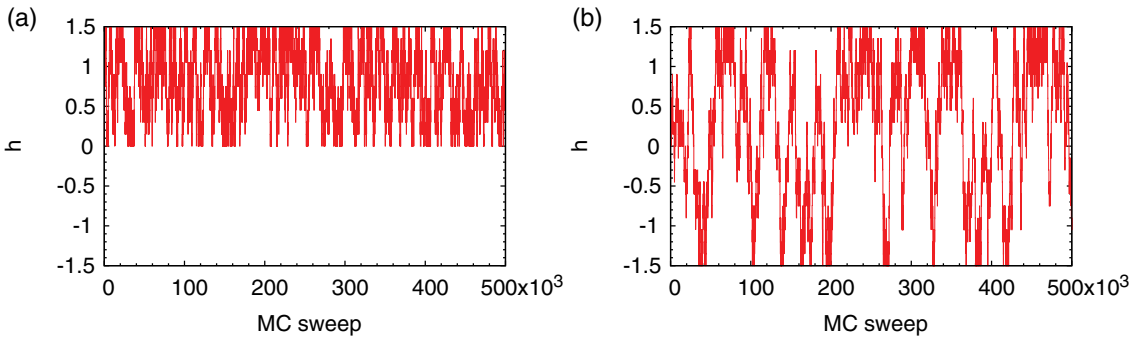

FIG. 14. (Color online) External field and MC sweep in the SM simulations (a) under T_c ($T = 1.97$) and (b) above T_c ($T = 3.88$). The linear lattice size L is 20.

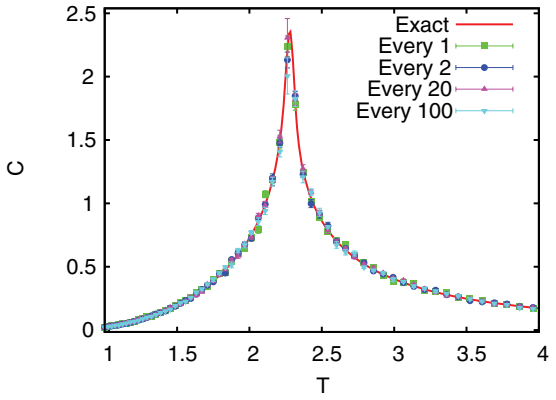

FIG. 15. (Color online) Heat capacity per spin C at $h = 0$. The linear lattice size L is 80. As shown in the legend, green squares, blue circles, purple triangles, and light-blue inverse triangles represent one parameter-updating attempt being made every 1, 2, 20, and 100 MC sweeps, respectively. The exact result (red solid line) was obtained by Berg's program [30] based on Ref. [33].

desirable to develop an even more efficient method for the STM free-energy estimation than the present ones.

C. Simulated magnetizing

We study the compatibility of ST with the first-order phase transition with external field changes by performing simulated magnetizing (SM) simulations, in which the temperature is fixed and the external field is updated by the Metropolis criterion. Figure 13 shows the external field as a function of the MC sweep in the SM simulations below T_c. We performed SM simulations in a number of lattice sizes from 2×2 to 20×20. These graphs illustrate the fact that as the system size becomes larger, the difficulty in simulations grows. In fact, it finally became impossible to observe the events in which the magnetization goes to the other side across the zero point [see Fig. 14(a)], while it was still possible above T_c [see Fig. 14(b)]. These results imply that the full range random walk happens above T_c but not below T_c. Therefore, this result suggests that

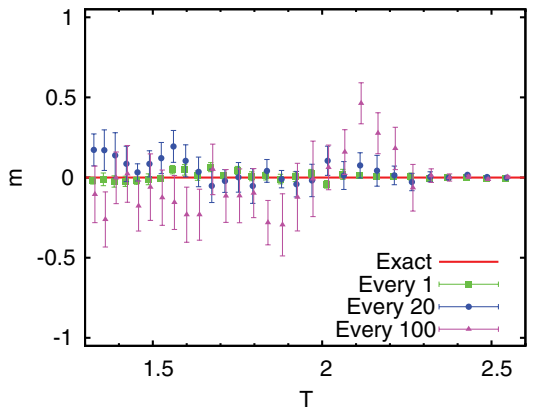

FIG. 16. (Color online) Magnetization per spin m for $h = 0$. As shown in the legend, green squares, blue circles, and purple triangles represent one parameter-updating attempt being made every 1, 20, and 100 MC sweeps, respectively. Some error bars were slightly shifted horizontally to aid the eye.

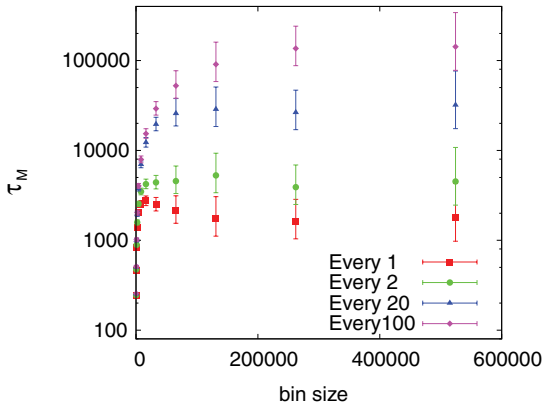

FIG. 17. (Color online) Correlation time analysis. Error bars show the 95% confident interval.

the random walk of temperature is crucial for the full range random walk of the external field. The full range random walk of the external field happens in the STM simulation when the temperature is high above T_c. Note that the Ising model is equivalent to the lattice gas model [31]. Hence, what happens in STM simulations can be understood as follows: Even though the phase transitions between gas and liquid do not directly occur, they do occur through the supercritical water region.

To explore this phenomenon more clearly, readers are referred to Ref. [32], which shows how the temperature and external field change during the STM simulation.

D. Frequency of temperature or external field updates

A common question about this kind of simulation is how frequently the parameter-updating attempts should be made. We want to emphasize that as long as the detailed balance condition is satisfied, the simulations should be correctly carried out.

We compared STM simulations performed with different parameter-updating frequencies. Figure 15 shows the results of the heat capacity as a function of temperature at $h = 0$, which were obtained by the STM method with different conditions. The conditions are one parameter-updating attempt every 1, 2, 20, and 100 MC sweeps. They show good agreement with each other. The error bars were obtained by the jackknife

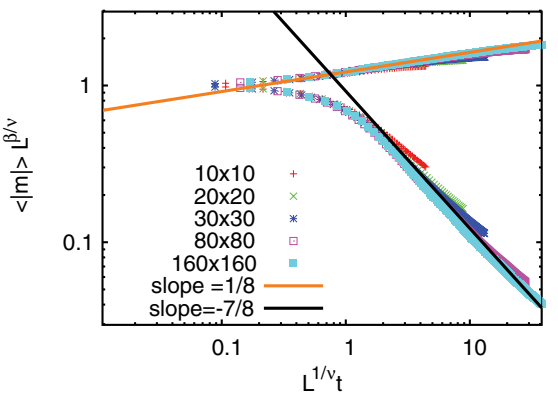

FIG. 18. (Color online) Scaled m for $h = 0$. The lines are the same as those used in Ref. [36].

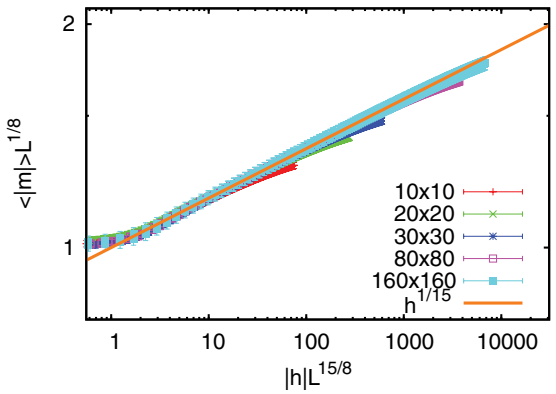

FIG. 19. (Color online) Scaled m at $T = T_c$.

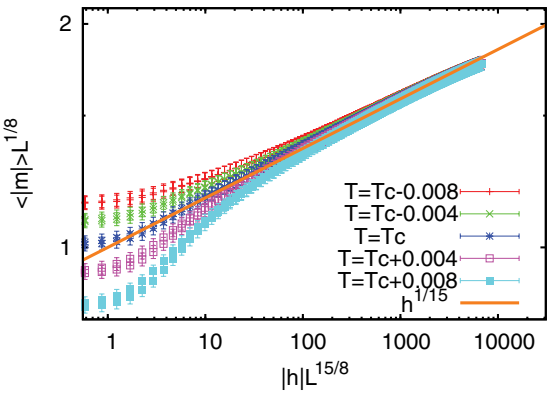

FIG. 21. (Color online) Scaled m near $T = T_c$.

method [29,30]. Note that the error bars tend to be larger as the parameter-updating frequency becomes less.

Figure 16 shows the magnetization as a function of temperature at $h = 0$. Data were obtained with several parameter-updating frequencies, such as one parameter-updating attempt every 1, 20, and 100 MC sweeps. They also agree with each other. Note that because finite sizes are employed, the magnetization under T_c at $h = 0$ is also zero. With the lower parameter-updating frequency, the convergence was not so good and the error bars tend to be larger. The error bars were obtained by the jackknife method [29,30]. These results suggest that the frequent parameter update does not make any artifacts and that it should be recommended.

Figure 17 shows the integrated correlation time of magnetization obtained at different parameter-updating frequencies. The height of data is expected to converge to the integrated correlation time between samples. This was calculated by using the jackknife method with different bin sizes [29,30]. Data were stored every ten MC sweeps. Thus the correlation time measured by one MC sweep should be ten times larger. The error bars were obtained with the χ^2 distribution. These results suggest that the higher the parameter-updating frequency employed, the shorter the correlation time obtained. Therefore, frequent parameter updates are preferred. Note that the observation that the frequent parameter updates are preferable is in accord with the statement that frequent replica-exchanging attempts are recommended [34,35].

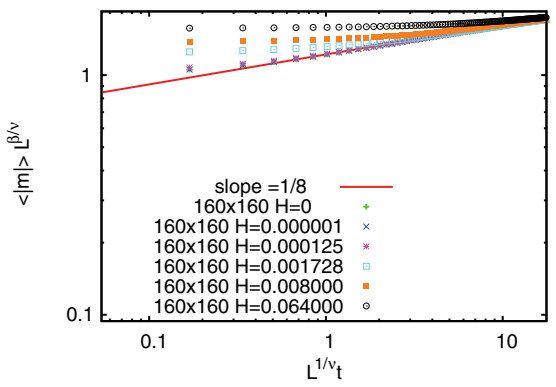

FIG. 20. (Color online) Scaled m near $h = 0$.

E. Observation of crossover

We study the crossover behavior of the phase transitions. We calculate the magnetization by the MBAR estimator around the critical point.

We employ the finite-size scaling approach, which is discussed in Ref. [36]. The scaling form of magnetization m with respect to the temperature and external field is given by

$$mL^{\beta/\nu} = \Psi(L^{1/\nu}t, L^{(\gamma+\beta)/\nu}h), \tag{23}$$

where $t = |T - T_c|/T_c$ and L is the linear size of the lattice. The Greek letters ν and γ stand for critical exponents. In the two-dimensional Ising model, $\beta = 1/8$, $\delta = 15$, $\nu = 1$, and $\gamma = 7/4$.

First we examine the scaling behavior of the magnetization. Figures 18 and 19 show the magnetization as functions of T and h, respectively, and we see that it obeys the critical behavior of $m \sim |T - T_c|^{\beta}$ and $|h|^{1/\delta}$, respectively. According to the scaling approach, when Lt or $L^{15/8}h$ is large enough, the finite effect can be negligible. In this case, Figs. 18 and 19 imply that those conditions are given by $Lt > 0.2$ and $L^{15/8}h > 1.1$, respectively.

We now study the behavior under conditions slightly different from the critical point. Figure 20 shows the magnetization as a function of temperature near $h = 0$. As the external field increases, the behavior differentiates in the low-temperature region. Even in the presence of a weak external field, the magnetization obeys $t^{1/8}$ when the temperature is relatively high enough. However, with a relatively strong external field, the scaling behavior disappears.

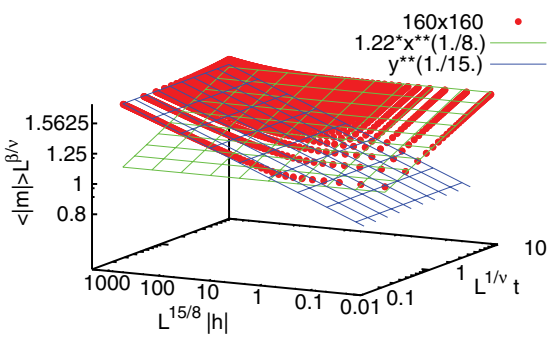

FIG. 22. (Color) Scaled m about the critical point. The linear lattice size $L = 160$. We display only the results for $T < T_c$.

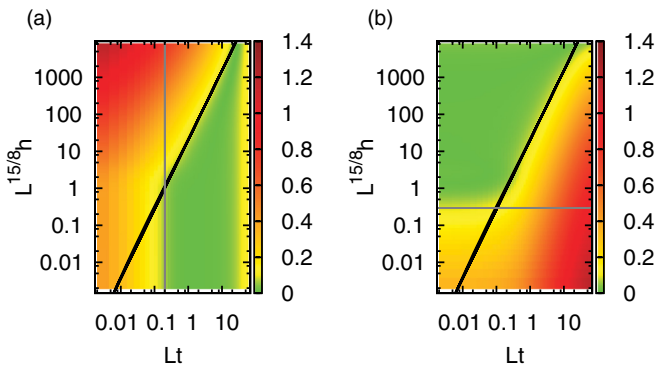

FIG. 23. (Color) Difference between magnetization and its expected scaling behavior about the critical point. The linear lattice size $L = 160$. (a) $|mL^{1/8} - 1.22(Lt)^{1/8}|$ is illustrated. The black line is $t = 0.2h^{8/15}$ and the vertical gray line is $Lt = 0.2$. (b) $|mL^{1/8} - (L^{15/8}h)^{1/15}|$ is illustrated. The black line is $t = 0.2h^{8/15}$ and the horizontal gray line is $L^{15/8}h = 0.3$

Figure 21 shows the magnetization as a function of the external field near $T = T_c$. As the temperature deviates from T_c, the behavior differentiates in the weak external field region. Thus, even with a slight difference from T_c, the magnetization obeys $h^{1/15}$ when the external field is strong enough.

Figure 22 illustrates the comprehensive behavior of $\langle|m|\rangle$ near the critical point. Note that this is a logarithmic scale plot. Near the h axis $\langle|m|\rangle$ obeys $|h|^{1/15}$ and near the T axis $\langle|m|\rangle$ obeys $|t|^{1/8}$.

Figures 23(a) and 23(b) show the difference between $\langle|m|\rangle L^{1/8}$ and $1.22(Lt)^{1/8}$ and between $\langle|m|\rangle L^{1/8}$ and $(L^{15/8}h)^{1/15}$, respectively. These data were obtained by the (160×160)-lattice-size simulations. Note that the factor 1.22 comes from the exact solution [19,37]. According to the crossover scaling formalism [38], if $t^{-15/8}h$ is large enough, then the magnetization obeys $m \sim t^{1/8}$, and if $h^{-8/15}t$ is large enough ($t^{-15/8}h$ is small enough), then it obeys $m \sim h^{1/15}$. Figure 23(a) shows that if the finite-size effects are negligible ($Lt \gg 0.2$) and $t \gg 0.2h^{8/15}$ (i.e., $th^{-8/15}$ is large), then the critical behavior is $m \sim t^{1/8}$. Figure 23(b) shows that if finite-size effects are negligible ($L^{15/8}h \gg 0.3$) and $t \ll 0.2h^{8/15}$ (i.e., $t^{-15/8}h$ is large), then the critical behavior is $m \sim h^{1/15}$. Thus Fig. 23 clearly shows that the line $t = 0.2h^{8/15}$ gives the boundary of the two scaling regimes.

IV. CONCLUSION

We have introduced two-dimensional simulated tempering in temperature and an external field, which we refer to as simulated tempering and magnetizing. We applied it to the two-dimensional Ising model. During the simulations, two-dimensional random walks in temperature and external field were realized. The random walk covered a wide area of temperature and external field so that the STM simulations enabled us to study a wide area of the phase diagram from a single simulation run.

Even though the first-order phase transitions with the external field change did not directly occur, the transitions happened through high-temperature regions, or supercritical water regions. The dimensional extension allowed us to overcome the difficultly of the first-order phase transitions. Thus this result suggests that the dimensional extension allows us to overcome the difficulty of crossing the first-order phase-transition points with the ST method. The similarity between ST and the REM implies that the dimensional extension of the REM will also give this property (an example is shown for the case of a two-dimensional REM simulation in temperature and pressure in Ref. [3]).

We also performed STM simulations with several different parameter-updating frequencies. According to the convergence and sizes of error bars, the more frequent attempts should be the better choice. The calculated autocorrelation time also suggested that frequents attempts are favorable.

We investigated the crossover behavior of phase transitions by calculating the magnetization per spin m around the critical point by the reweighting techniques. The results showed agreement with previous theoretical studies. This supports the validity of the two-dimensional ST method, or STM.

With the data of the present work, we can calculate the two-dimensional density of states $n(E,M)$ so that we can determine the weight factor for the two-dimensional multicanonical simulations. Therefore, we can also perform the two-dimensional multicanonical simulations. The STM method will be very useful for simulating spin-glass systems. We also remark that the present methods are useful for not only spin systems but also other complex systems with many degrees of freedom. It is worth noting that because this method does not modify the energy calculation, the method should be very much compatible with existing package programs.

ACKNOWLEDGMENTS

We thank Wolfhard Janke, Desmond Johnston, and Thomas Neuhaus for useful discussions. Some of the computations were performed on the supercomputers at the Information Technology Center, Nagoya University, at the Research Center for Computational Science, Institute for Molecular Science, and at the Supercomputer Center, Institute for Solid State Physics, University of Tokyo. This work was supported in part by Japan Society for the Promotion of Science Institutional Program for Young Researcher Overseas Visit (T.N.) and by Grants-in-Aid for Scientific Research on Innovative Areas ("Fluctuations and Biological Functions") and for the Next Generation Super Computing Project, Nanoscience Program, and Computational Materials Science Initiative from the Ministry of Education, Culture, Sports, Science and Technology, Japan.

APPENDIX: LATTICE GAS AND ISING MODEL

The total energy of Ising model H on a square lattice can be converted into that of lattice gas in the following manner:

$$H = -J\sum_{\langle i,j\rangle}\sigma_i\sigma_j - h\sum\sigma_i$$
$$= -J\sum_{\langle i,j\rangle}(2s_i - 1)(2s_j - 1) - h\sum(2s_i - 1), \quad \text{(A1)}$$

where $\sigma_i = \pm 1$ and $s_i = 1,0$. If $\sigma_i = 1$, then $s_i = 1$ and vice versa. We then have

$$H = -4J \sum_{\langle i,j \rangle} s_i s_j + 2J \sum_{\langle i,j \rangle} (s_i + s_j) + J \sum_{\langle i,j \rangle} 1 - h \sum (2s_i - 1)$$
$$= -4J \sum_{\langle i,j \rangle} s_i s_j + 8Jn + 2JN - 2hn + hN = -4J \sum_{\langle i,j \rangle} s_i s_j - (2h - 8J)n + (h - 2J)N, \tag{A2}$$

where n and N are the number of occupied sites and the total number of sites, respectively. The first term corresponds to the attractive energy between particles of lattice gas. The second term corresponds to the chemical potential of lattice gas. The last term is a constant. Here, we define $\mu \equiv (2h - 8J)$ and $E_g \equiv -4J \sum_{\langle i,j \rangle} s_i s_j$.

Thus, free energy per spin f is given by

$$\exp(-\beta f N) = \sum_{\sigma_0 = \pm 1; \sigma_1 = \pm 1, \ldots, \sigma_N = \pm 1} \exp(-\beta H)$$
$$= \sum_{s_0 = 1,0; s_1 = 1,0, \ldots, s_N = 1,0} \exp[-\beta(E_g - \mu n)] \exp[-\beta(h - 2J)N] = \Theta \exp[-\beta(h - 2J)N]$$
$$= \exp(\beta p N) \exp[-\beta(h - 2J)N], \tag{A3}$$

where p is pressure. Instead of V, N appears. The Greek letter Θ stands for the Grand partition function, where $\Theta = \sum_{s_0 = 1,0; s_1 = 1,0, \ldots, s_N = 1,0} \exp[-\beta(E_g - \mu n)]$. The last two equations were obtained with grand canonical ensembles. Therefore, we obtain

$$-f = p - (h - 2J), \tag{A4}$$
$$p = h - f - 2J. \tag{A5}$$

Thus, we conclude that the canonical ensemble of Ising model is equivalent to the μ-T ensemble of lattice gas model with the following correspondence:

$$p = h - f - 2J, \tag{A6}$$
$$\mu = (2h - 8J), \tag{A7}$$
$$E_g = -4J \sum_{\langle i,j \rangle} s_i s_j. \tag{A8}$$

[1] U. H. E. Hansmann and Y. Okamoto, in *Annual Reviews of Computational Physics VI*, edited by D. Stauffer (World Scientific, Singapore, 1999), pp. 129–157.

[2] A. Mitsutake, Y. Sugita, and Y. Okamoto, Biopolymers **60**, 96 (2001).

[3] Y. Sugita and Y. Okamoto, in *Lecture Notes in Computational Science and Engineering*, edited by T. Schlick and H. H. Gan (Springer, Berlin, 2002), pp. 304–332; arXiv:cond-mat/0102296.

[4] B. A. Berg and T. Neuhaus, Phys. Lett. B **267**, 249 (1991).

[5] B. A. Berg and T. Neuhaus, Phys. Rev. Lett. **68**, 9 (1992).

[6] A. P. Lyubartsev, A. A. Martsinovski, S. V. Shevkunov, and P. N. Vorontsov-Velyaminov, J. Chem. Phys. **96**, 1776 (1992).

[7] E. Marinari and G. Parisi, Europhys. Lett. **19**, 451 (1992).

[8] K. Hukushima and K. Nemoto, J. Phys. Soc. Jpn. **65**, 1604 (1996).

[9] C. J. Geyer, in *Computing Science and Statistics, Proceedings of the 23rd Symposium on the Interface*, edited by E. M. Keramidas (Interface Foundation of North America, Fairfax Station, VA, 1991), pp. 156–163.

[10] F. Wang and D. P. Landau, Phys. Rev. Lett. **86**, 2050 (2001).

[11] F. Wang and D. P. Landau, Phys. Rev. E **64**, 056101 (2001).

[12] A. Laio and M. Parrinello, Proc. Natl. Acad. Sci. USA **99**, 12562 (2002).

[13] R. H. Swendsen and J.-S. Wang, Phys. Rev. Lett. **57**, 2607 (1986).

[14] Y. Iba, Int. J. Mod. Phys. C **12**, 623 (2001).

[15] J. Kim and J. E. Straub, J. Chem. Phys. **133**, 154101 (2010).

[16] A. Mitsutake and Y. Okamoto, Phys. Rev. E **79**, 047701 (2009).

[17] A. Mitsutake and Y. Okamoto, J. Chem. Phys. **130**, 214105 (2009).

[18] A. Mitsutake, J. Chem. Phys. **131**, 094105 (2009).

[19] D. S. Gaunt and C. Domb, J. Phys. C **3**, 1442 (1970).

[20] J. D. Chodera and M. R. Shirts, J. Chem. Phys. **135**, 194110 (2011).

[21] C. Zhang and J. Ma, J. Chem. Phys. **132**, 244101 (2010).

[22] M. Matsumoto and T. Nishimura, ACM Trans. Model. Comput. Simul. **8**, 3 (1998).

[23] A. Mitsutake and Y. Okamoto, Chem. Phys. Lett. **332**, 131 (2000).

[24] A. M. Ferrenberg and R. H. Swendsen, Phys. Rev. Lett. **63**, 1195 (1989).

[25] S. Kumar, J. M. Rosenberg, D. Bouzida, R. H. Swendsen, and P. A. Kollman, J. Comput. Chem. **13**, 1011 (1992).
[26] M. R. Shirts and J. D. Chodera, J. Chem. Phys. **129**, 124105 (2008).
[27] A. Mitsutake, Y. Sugita, and Y. Okamoto, J. Chem. Phys. **118**, 6664 (2003).
[28] K. Binder, Z. Phys. B **43**, 119 (1981).
[29] R. G. Miller, Biometrika **61**, 1 (1974).
[30] B. A. Berg, *Markov Chain Monte Carlo Simulations and Their Statistical Analysis* (World Scientific, Singapore, 2004).
[31] T. D. Lee and C. N. Yang, Phys. Rev. **87**, 410 (1952).
[32] See Supplemental Material at http://link.aps.org/supplemental/10.1103/PhysRevE.86.056705 for looking into the behavior of T and h during the STM simulation.
[33] A. E. Ferdinand and M. E. Fisher, Phys. Rev. **185**, 832 (1969).
[34] D. J. Sindhikara, Y. Meng, and A. E. Roitberg, J. Chem. Phys. **128**, 024103 (2008).
[35] D. J. Sindhikara, D. J. Emerson, and A. E. Roitberg, J. Chem. Theor. Comput. **6**, 2804 (2010).
[36] D. P. Landau, Phys. Rev. B **13**, 2997 (1976).
[37] C. N. Yang, Phys. Rev. **85**, 808 (1952).
[38] M. E. Fisher, Rev. Mod. Phys. **46**, 597 (1974).